Laser scattering on an atmospheric pressure plasma jet : disentangling Rayleigh, Raman and Thomson scattering

Laser scattering on an atmospheric pressure plasma jet: disentangling Rayleigh, Raman and Thomson scattering

2012 Plasma Sources Sci. Technol. 21 015003

(http://iopscience.iop.org/0963-0252/21/1/015003)

Plasma Sources Sci. Technol. **21** (2012) 015003 (9pp) doi:10.1088/0963-0252/21/1/015003

Laser scattering on an atmospheric pressure plasma jet: disentangling Rayleigh, Raman and Thomson scattering

A F H van Gessel, E A D Carbone, P J Bruggeman and J J A M van der Mullen

Eindhoven University of Technology, Department of Applied Physics, PO Box 513, 5600 MB, Eindhoven, The Netherlands

E-mail: a.f.h.v.gessel@tue.nl

Received 21 June 2011, in final form 8 November 2011
Published 31 January 2012
Online at stacks.iop.org/PSST/21/015003

Abstract
Laser scattering provides a very direct method for measuring the local densities and temperatures inside a plasma. We present new experimental results of laser scattering on an argon atmospheric pressure microwave plasma jet operating in an air environment. The plasma is very small so a high spatial resolution is required to study the effect of the penetration of air molecules into the plasma. The scattering signal has three overlapping contributions: Rayleigh scattering from heavy particles, Thomson scattering from free electrons and Raman scattering from molecules. The Rayleigh scattering signal is filtered out optically with a triple grating spectrometer. The disentanglement of the Thomson and Raman signals is done with a newly designed fitting method. With a single measurement we determine profiles of the electron temperature, electron density, gas temperature, partial air pressure and the N_2/O_2 ratio, with a spatial resolution of 50 μm, and including absolute calibration.

(Some figures may appear in colour only in the online journal)

1. Introduction

Non-thermal atmospheric pressure plasmas have a wide range of applications, including surface modification [1], chemical conversion and synthesis [2], sterilization and wound healing [3, 4]. They do not require a complicated vacuum system, which makes them cheaper and more practical. However, this inevitably means that the plasma is in contact with air. Even when the plasma is created inside a jet of a controlled gas (usually argon), there will always be a finite amount of air entrainment into the plasma. This significantly increases the complexity of the plasma physics and chemistry. The focus of this paper is the air entrainment into an atmospheric pressure plasma jet.

In addition to the increased complexity another problem in the diagnostics of atmospheric pressure plasmas is their size. Many plasma jets have typical radial sizes of less than 1 mm, and these microplasmas consequently have steep gradients. This requires a very high spatial resolution in the measurements.

We use laser scattering, as this diagnostic is a good candidate for obtaining these high spatial resolutions. The laser can be focused to a small spot, and one does not have to worry about line-of-sight problems, as in optical emission spectroscopy. The different species in the plasma, such as electrons and heavy particles, are probed directly by the laser, providing a reliable method for measuring densities and temperatures. This was shown recently for these non-thermal plasmas by Palomares *et al* [5].

Three types of laser scattering can be distinguished. First, *Rayleigh scattering*, the elastic scattering of photons on electrons bound to heavy particles, is used to measure the gas temperature T_g [5–8]. Second, *Thomson scattering*, the elastic scattering on free electrons, is employed to measure the electron density n_e and electron temperature T_e [5, 7–10]. And third, *Raman scattering*, inelastic scattering on molecules such as O_2 and N_2, which gives the molecular densities n_{O_2} and n_{N_2} and the rotational temperature T_{rot} [11, 12]. Moreover, Raman scattering will also be used for calibration [5].

In order to measure the Thomson signal, care must be taken to filter out the much stronger Rayleigh signal. An established method is to do this optically with a triple grating spectrometer (TGS), which acts as a notch filter to remove the Rayleigh signal.

The Raman signal and the Thomson signal cannot be separated with a TGS, because their spectra cover the same spectral range. Consequently, laser scattering is mostly applied in situations where there is either scattering on electrons (Thomson scattering), or on molecules (Raman scattering), not both. The problem of measuring a Thomson signal in Raman active plasmas has been recognized by Narishige *et al* [13]. Their spectral resolution was not sufficient to resolve the rotational lines of the Raman spectrum. Therefore, they could not distinguish between the Raman and the Thomson signal directly. Instead they isolated the Thomson signal from the Raman signal using the differences in the scattering characteristics depending on the scattering wavelength and scattering geometry. This method requires a flexible setup to measure at different laser wavelengths and scattering angles. When using a TGS this is experimentally difficult because a TGS is generally designed for one particular laser wavelength, and is also not easily movable. Furthermore, the information about the plasma in the Raman signal is not utilized.

We present a new method for disentangling the contributions of Thomson and Raman scattering to the measured signal with a newly designed fitting procedure. From a single measurement we can obtain spatially resolved n_e and T_e from the Thomson signal, and n_{O_2}, n_{N_2} and T_{rot} from the Raman signal. Using this method we show new measurements of Rayleigh, Thomson and Raman scattering of an atmospheric pressure microwave plasma jet, with a spatial resolution of 50 μm.

In the next section we describe in detail the different types of laser scattering. In section 3 the experimental setup and the fitting method are discussed, followed by the results in section 4. The applicability and limitations of the technique are discussed in section 5. The last section contains a small summary.

2. Laser scattering

When a laser beam is guided through a plasma and the scattered light is detected, the measured scattered power per unit of wavelength P_λ[1] can in general be given by [14, 15]

$$P_\lambda = f L P_i \Delta\Omega \cdot n \cdot \frac{\mathrm{d}\sigma}{\mathrm{d}\Omega} \cdot S_\lambda(\lambda), \tag{1}$$

where f is a constant factor that takes into account the efficiency of the optics and camera, L the length of the detection volume along the laser path, P_i the incident laser power, $\Delta\Omega$ the solid angle of detection, n the density of the scattering particle, and $\mathrm{d}\sigma/\mathrm{d}\Omega$ the differential cross section. The factor $S_\lambda(\lambda)$ includes the spectral distribution as a function of wavelength, which consists of the instrumental profile (in the case of Rayleigh and Raman scattering), or a broadened line profile (in the case of Thomson scattering). It is normalized such that $\int S_\lambda(\lambda)\mathrm{d}\lambda = 1$.

[1] The subscript λ denotes that the quantity is per unit of wavelength. The wavelength integrated value is written without subscript, so $P = \int P_\lambda \,\mathrm{d}\lambda$.

2.1. Rayleigh scattering

The Rayleigh scattering signal is proportional to the density of heavy particles n_h, which, by applying the ideal gas law $p = n_h k_B T_g$, is inversely proportional to the gas temperature T_g at constant given pressure p. To find an absolute T_g, the measurement must be calibrated with a reference measurement at known temperature T_{ref}, so

$$T_g = \frac{P_{ref}}{P_{plas}} T_{ref}, \tag{2}$$

where P_{plas} and P_{ref} are the wavelength integrated scattered power of the Rayleigh signal of the plasma and the reference measurement, respectively.

The differential cross section $\mathrm{d}\sigma_{ray}/\mathrm{d}\Omega$ for Rayleigh scattering depends on the species [16], which means that the reference measurement should in principle be done with the same gas composition. In our experiments we made reference measurements with the gas flow on, and the plasma off, assuming room temperature. The cross sections of argon and air are very similar: $5.4 \times 10^{-32}\,\mathrm{m}^2$ for argon versus $6.2 \times 10^{-32}\,\mathrm{m}^2$ and $5.3 \times 10^{-32}\,\mathrm{m}^2$ for N_2 and O_2, respectively [17]. A small change in the gas composition is therefore not critical.

Rayleigh scattering has a negligible broadening compared with the instrumental profile of the spectrometer, so that $S_\lambda(\lambda)$ is equal to the instrumental profile.

2.2. Thomson scattering

The Thomson signal is Doppler broadened due to the velocity of the electrons. Thomson scattering is incoherent if the scattering parameter $\alpha \ll 1$ [15]. In our case with $T_e \approx 2\,\mathrm{eV}$ and $n_e \approx 10^{20}\,\mathrm{m}^{-3}$ as typical conditions, $\alpha \approx 0.06$, which means that the scattering can be considered incoherent. With incoherent Thomson scattering and a Maxwellian velocity distribution, this leads to a Gaussian profile centred at the laser wavelength λ_i [15],

$$S_\lambda(\lambda) = \frac{1}{\Delta\lambda\sqrt{\pi}} \mathrm{e}^{-\left(\frac{\lambda-\lambda_i}{\Delta\lambda}\right)^2}, \tag{3}$$

where $\Delta\lambda$ is the $1/e$ width of the Gaussian profile. $\Delta\lambda$ can be related to T_e with [7, 15],

$$T_e = \frac{m_e c^2}{4k_B} \cdot \left(\frac{\Delta\lambda}{\lambda_i}\right)^2, \tag{4}$$

for a perpendicular scattering angle. In this equation m_e is the electron mass, c the speed of light and k_B the Boltzmann constant.

For perpendicular Thomson scattering the differential cross section is [15]

$$\frac{\mathrm{d}\sigma_{th}}{\mathrm{d}\Omega} = r_e^2 \tag{5}$$

Table 1. Molecular constants, after Penney *et al* [18], except E_{10}, which is after Herzberg [19].

Species		N_2	O_2
B	(eV)	2.467×10^{-4}	1.783×10^{-4}
γ^2	(F^2m^4)	3.95×10^{-83}	1.02×10^{-82}
g_J	(J odd/even)	3/6	1/0
I		1	0
E_{10}	(eV)	0.289	0.193

with $r_e = 2.818 \times 10^{-15}$ m the classical electron radius. To determine the electron density n_e with equation (1), the measurement must be absolutely calibrated (i.e. $fLP_i\Delta\Omega$ must be determined). This is done by means of Raman scattering on ambient air at atmospheric pressure and room temperature.

2.3. Rotational Raman scattering

In Raman scattering the scattered wavelength changes due to an associated transition in the rotational or vibrational state of a molecule. Because of the range of our spectrometer we consider only rotational Raman scattering. The following is described in detail by Penney *et al* [18] and Van de Sande [15].

The transitions from rotational quantum number J to J' lead to peaks in the spectrum at different wavelengths:

$$\lambda_{J\to J'} = \lambda_i + \frac{\lambda_i^2}{hc} \cdot B\left(\left(J'^2 + J'\right) - \left(J^2 + J\right)\right), \qquad (6)$$

where h is Planck's constant and B the rotational constant which is species dependent (table 1). The allowed transitions are those given by $J' = J + 2$ (Stokes) and $J' = J - 2$ (anti-Stokes). The (wavelength integrated) scattered power of each peak is proportional to the product of density and the corresponding differential cross section, that is

$$P_{J\to J'} \propto n_J \cdot \frac{d\sigma_{J\to J'}}{d\Omega}. \qquad (7)$$

The differential cross section for perpendicular scattering can be written as

$$\frac{d\sigma_{J\to J'}}{d\Omega} = \frac{64\pi^4}{45\epsilon_0^2} \cdot b_{J\to J'} \cdot \frac{\gamma^2}{\lambda_{J\to J'}^4}, \qquad (8)$$

with ϵ_0 the vacuum permittivity, γ^2 the anisotropy of the molecular-polarizability tensor (see table 1) and $b_{J\to J'}$ the Placzek–Teller coefficients, given by

$$b_{J\to J'} = \frac{3\left(J + J'\right)\left(J + J' + 2\right)}{8\left(2J + 1\right)\left(J + J' + 1\right)}. \qquad (9)$$

We assume that the density of states J follows a Boltzmann distribution depending on the rotational temperature T_{rot}, such that

$$n_J = \frac{n_{mol}}{Q} \cdot g_J\left(2J + 1\right) e^{-\frac{BJ(J+1)}{k_B T_{rot}}}, \qquad (10)$$

with n_{mol} the molecular density, g_J the statistical weight factor (table 1), and Q the partition sum that can be approximated by

$$Q \approx (2I + 1)^2 \frac{k_B T_{rot}}{2B}. \qquad (11)$$

Here I is the nuclear spin quantum number (table 1).

Following equation (1) the total measured Raman spectrum is given by

$$P_\lambda(\lambda) = fLP_i\Delta\Omega \cdot \sum_{J'=J\pm2} n_J \frac{d\sigma_{J\to J'}}{d\Omega} S_\lambda(\lambda - \lambda_{J\to J'}). \qquad (12)$$

Under our experimental conditions the broadening of the rotational lines is negligible compared with the instrumental broadening. Therefore, in this case $S_\lambda(\lambda - \lambda_{J\to J'})$ can be taken equal to the instrumental profile, centered at $\lambda_{J\to J'}$.

3. Experiment

We used a microwave surfatron operating at a frequency of 2.45 GHz to create a plasma in a ceramic tube (Al_2O_3) with an inner diameter of 0.8 mm, ending in air (see figure 1). Through the tube argon is flushed with a flow rate of 1.0 slm, which results in a flow speed of 33 m s^{-1}. The flow can be characterized by a Reynolds number with a value of about 2000. This means that inside the tube the flow is expected to be laminar, but in the jet turbulent structures appear as a result of Kelvin–Helmholtz instabilities [20].

The same setup was used by Palomares *et al* [5], with the difference that in our case the surfatron launcher is cooled with a flow of 20 slm of air around the tube (figure 1).

The microwave generator produces a forward power of 50 W. However, the actual power absorbed by the plasma is less, which can be deduced from the fact that the surfatron launcher needs cooling. A considerable fraction of the power is dissipated in the launcher, and not in the plasma.

The laser scattering is done by focusing a pulsed laser inside the plasma. The laser (Edgewave IS6II-E) is a Nd : YAG laser operating at 532 nm. It has a pulse energy of 4 mJ and a repetition rate of 4 kHz. The scattered light is collected perpendicularly by two lenses that image the laser beam onto the entrance slit of a TGS. See also figure 1.

The entrance slit of the TGS is mounted horizontally, followed by a rotator to rotate the image to the vertical plane. The TGS essentially consists of two parts: the first part, consisting of the first and second grating (1800 grooves mm^{-1}) together with a mask, forms a *notch filter* to remove the central laser wavelength from the spectrum. An intermediate slit removes stray light caused by diffraction of the mask. At the same time this slit forms the entrance slit of the second part of the TGS, the *spectrometer*. The third grating (identical to the other two gratings) forms a spectrum that is focused onto an Andor DH534 iCCD camera. The optics in the TGS are designed such that the light onto the iCCD is a 1 : 1 image of the laser beam.

The mask is needed for Raman and Thomson measurements, to eliminate the much stronger Rayleigh signal and false stray light. To remove the false stray light even more, a blackened box is built around the TGS, and black screens are placed between the light paths.

When the mask is removed, the TGS acts as a normal spectrometer. This setting is used to measure the Rayleigh signal.

The spatial resolution along the laser beam is limited by the optics inside the TGS and is about 50 μm. Perpendicular

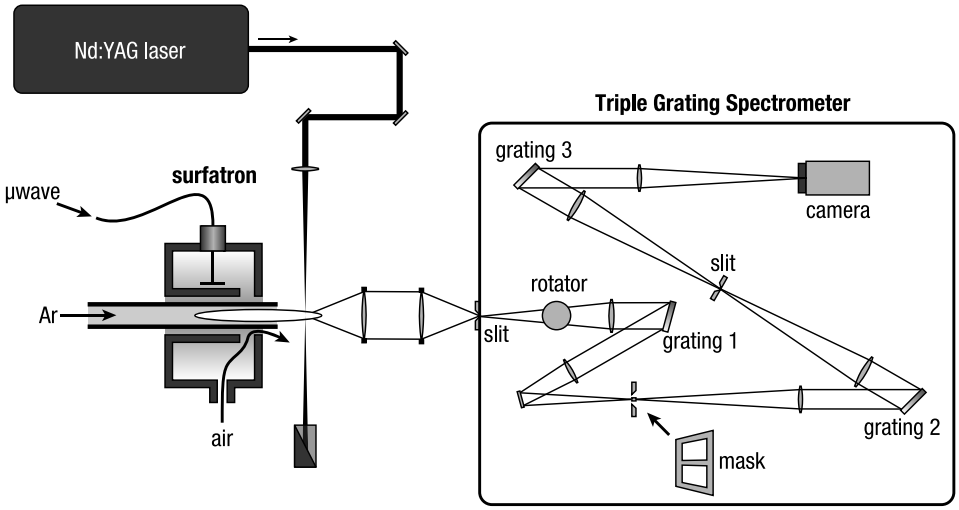

Figure 1. Experimental setup with the microwave surfatron launcher and the TGS. For clarity the surfatron jet is drawn horizontally, but in reality the jet was mounted vertically, perpendicular to the laser beam and the scattering direction.

to the laser beam the spatial resolution is determined by the beam waist, and is about 100 μm. The spectral resolution of the detection system is about 0.12 nm FWHM. The linewidth of the laser is 24 pm, which is much smaller.

3.1. Fitting procedure

Rayleigh scattering measurements (TGS without mask) are done separately, and since the signal has negligible broadening, there is no information about the plasma in the wavelength distribution. To find P_{plas} and P_{ref}, first the signal background is subtracted, then the spectrum is simply integrated. Since T_{ref} is known (room temperature), T_{g} can be calculated using equation (2).

In combined Thomson and Raman measurements (TGS with mask) we distinguish three contributions: due to Thomson scattering, Raman scattering on N_2 and Raman scattering on O_2. Under our experimental conditions, these contributions have similar intensities, and their spectra overlap. With specially designed software, written in Matlab®, we are able to fit these overlapping signals, and separate them.

To do the fitting we calculate the theoretical spectra as explained in section 2. The Rayleigh signal provides a suitable instrumental profile. The Raman spectra are thus calculated using equation (12) with $S_\lambda(\lambda - \lambda_{J\to J'})$ the normalized measured Rayleigh signal. The instrumental broadening is assumed to have a negligible effect on the Thomson signal, so no convolution is applied to the Thomson spectrum. The three contributions—Thomson, N_2-Raman and O_2-Raman—are calculated separately and summed. Also a constant background C is added. So for the total signal

$$P_{\lambda,\text{total}} = P_{\lambda,\text{thom}}(n_\text{e}, T_\text{e}) + P_{\lambda,\text{N}_2}(p_{\text{N}_2}, T_\text{rot}) + P_{\lambda,\text{O}_2}(p_{\text{O}_2}, T_\text{rot}) + C. \quad (13)$$

The experimental data is corrected for imaging errors of the TGS. The fitting of $P_{\lambda,\text{total}}$ is done by calculating the least square difference using the Matlab function `fminsearch`, which makes use of a multivariable search method by Lagarias *et al* [21].

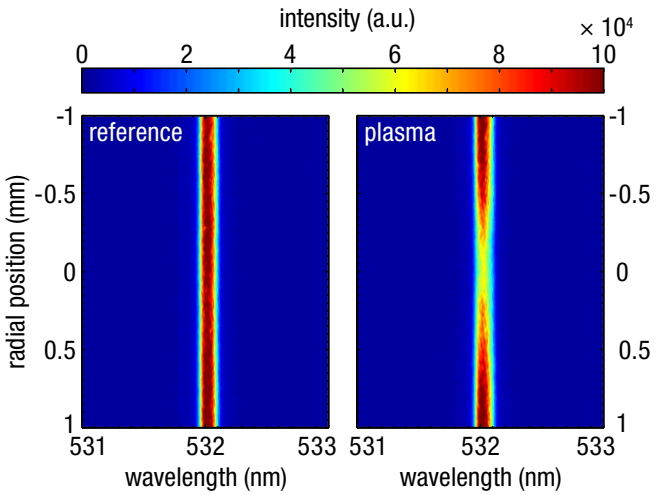

Figure 2. iCCD image of the Rayleigh reference measurement without plasma (left) and the Rayleigh scattering measurement in the plasma jet (right) at 4.75 mm from the tube end.

Instead of using the parameters p_{N_2} and p_{O_2}, it is more convenient to use the partial air pressure $p_{\text{N}_2} + p_{\text{O}_2}$, and the mixing ratio $p_{\text{N}_2}/p_{\text{O}_2}$ as fit parameters. The total number of fit parameters is 6: n_e, T_e, T_rot, $p_{\text{N}_2} + p_{\text{O}_2}$, $p_{\text{N}_2}/p_{\text{O}_2}$ and C.

To obtain absolute values of the pressure and densities, the signal must be absolutely calibrated. This is done by fitting a Raman spectrum of ambient air without plasma. In this case the temperature is fitted and the air pressure is known (10^5 Pa), and the experimental factors $f L P_i \Delta\Omega$ can be calculated.

4. Results

The Rayleigh measurement of the plasma and the reference measurement without plasma are shown in figure 2. The images are accumulated over 8000 laser shots (2 s) and show spectral information along the horizontal axis, and spatial information along the vertical axis. The spectrum is peaked at the laser wavelength. In the radial direction (along the laser

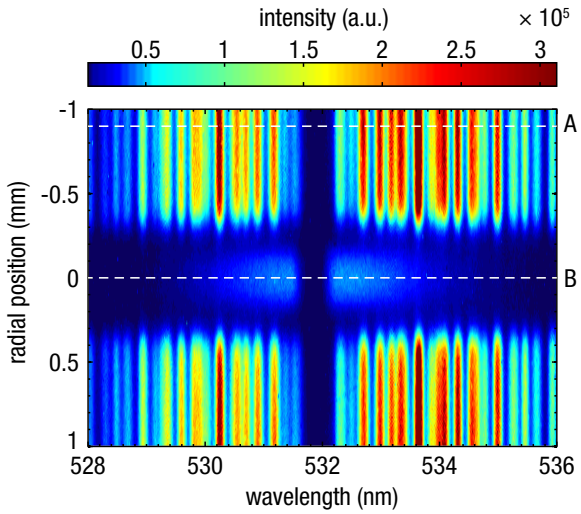

Figure 3. iCCD image of Thomson and Raman scattering in a microwave plasma jet, 1 mm from the tube end.

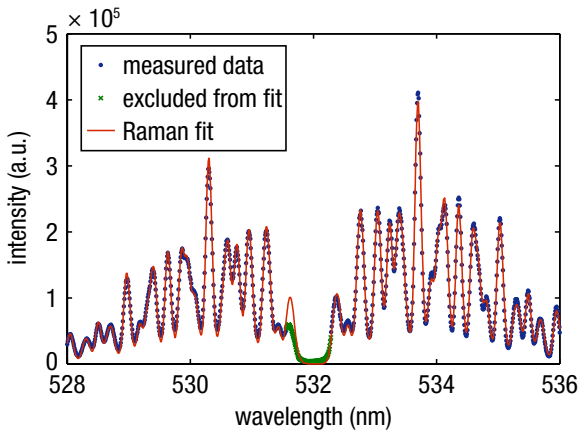

Figure 4. Raman spectrum of ambient air at position A in figure 3, used for absolute calibration. $p_{N_2+O_2}$ is fixed to 10^5 Pa. The fitted values are $T_{rot} = 308$ K and the ratio $N_2/O_2 = 79.8/20.2\%$.

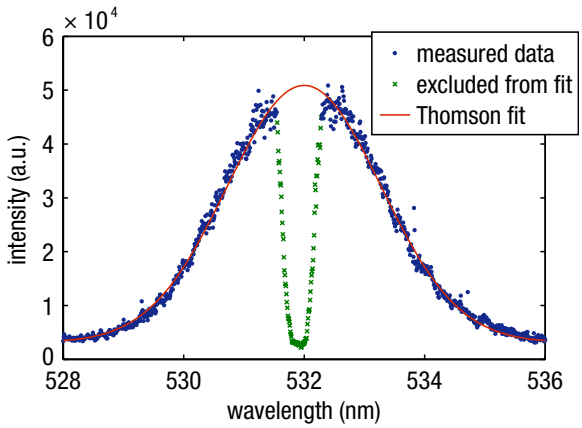

Figure 5. Thomson spectrum in the center of the plasma jet at position B in figure 3. The fitted values are $n_e = 4.6 \times 10^{20}$ m^{-3} and $T_e = 1.5$ eV.

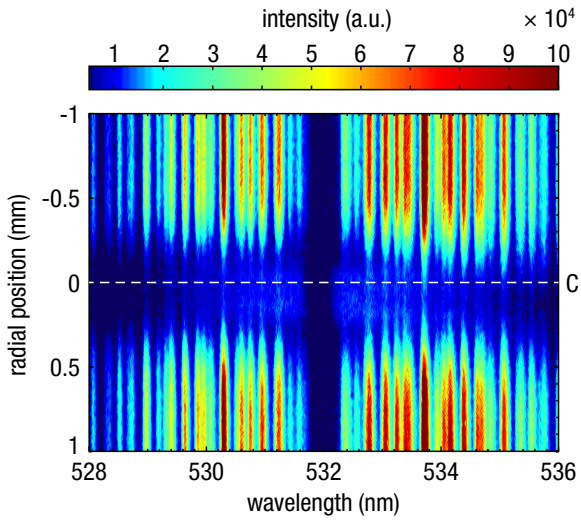

Figure 6. iCCD image of Thomson and Raman scattering in a microwave plasma jet, 4.75 mm from the tube end.

beam) the reference measurement shows almost no variation. This is due to the fact that the differential cross sections of argon and air are similar. In the measurement with plasma the signal decreases in the center due to higher temperatures. T_g is calculated at different radial positions, and is shown below in figure 13. The spectrum of the reference signal is used as instrumental profile in the fitting of the Raman spectra.

Figure 3 shows the iCCD image of a combined Raman and Thomson scattering measurement, taken at 1 mm from the tube end. The image is accumulated over 2×10^6 laser shots (10 min). In the center at 532 nm the part of the spectrum at the laser wavelength is missing due to the filtering of the TGS. Each horizontal cross section in the image gives a Raman or Thomson spectrum at different radial positions along the laser beam.

The horizontal cross section indicated with A at 0.9 mm radial position is shown in figure 4. This part is outside the plasma and outside the argon flow, and shows Raman scattering of ambient air and at atmospheric pressure. The fitted temperature of 308 K corresponds well to the room temperature (295 K), and the fitted N_2/O_2 value accurately matches the standard air conditions. The fit is used for absolute calibration.

Since the measurement is taken near the tube end there is only very little air entrainment into the flow. This is visible in the center of the argon flow due to the absence of a Raman signal. Instead a clear Gaussian Thomson signal is visible. This is shown in figure 5, which corresponds to the center of the plasma at cross section B. The central part of the spectrum is removed by the mask of the TGS. This part at the laser wavelength is excluded from the fitting.

Another iCCD image, taken further downstream at an axial position of 4.75 mm from the tube end, is shown in figure 6. In this image the air has penetrated into the argon flow, causing an overlapping Raman and Thomson signal in the center of the plasma. Cross section C corresponding to the center of the plasma is shown in figure 7, with a fit of the Raman and Thomson signal.

Similar fits are made at different cross sections of figure 6, at 4 pixels distance and each with 4 pixels binning. This corresponds to the maximum spatial resolution of the system of about 50 μm. The electron densities and temperatures obtained

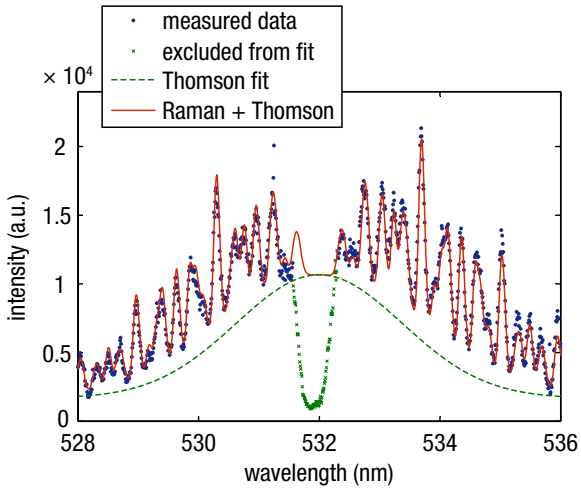

Figure 7. Overlapping Raman and Thomson scattering in the center of the plasma jet at position C in figure 6. The fitted values are $n_e = 1.8 \times 10^{20}$ m^{-3}, $T_e = 1.7$ eV, $T_{rot} = 386$ K, $p_{N_2+O_2} = 9.7 \times 10^3$ Pa and $N_2/O_2 = 80.2/19.8\%$.

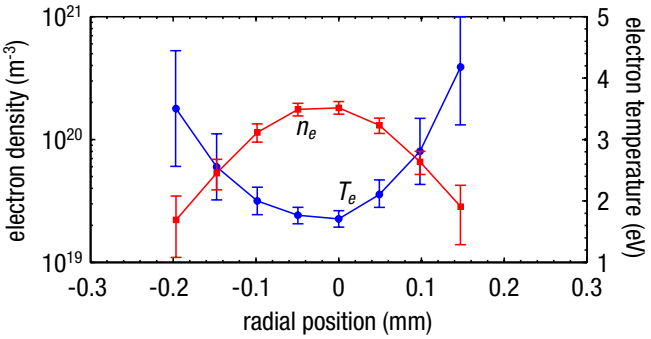

Figure 8. Electron temperature and density obtained at 4.75 mm from the tube end.

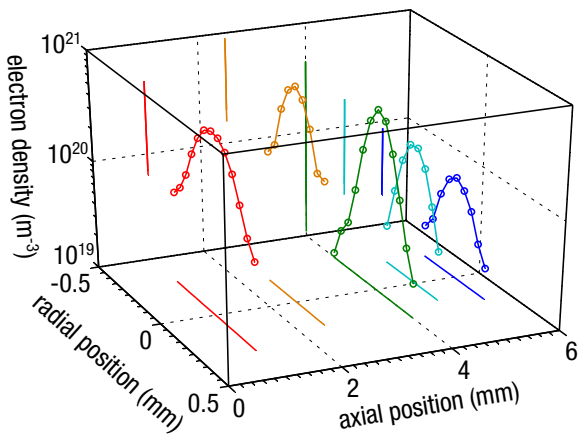

Figure 9. 2D profile of n_e of the plasma jet. Axial position 0 is defined at the tube end. An indication of the error bars is shown in figure 8.

by these fits are shown in figure 8. According to the Thomson signal the plasma has a width of about 0.4 mm.

Toward the edge n_e decreases, while T_e increases (this is discussed further in section 5.2). Figures 9 and 10 show 2D plots of radial profiles at different axial positions. Figure 9 suggests that n_e has a maximum axially at about 2 mm from the tube end. However, this is an artifact which most likely

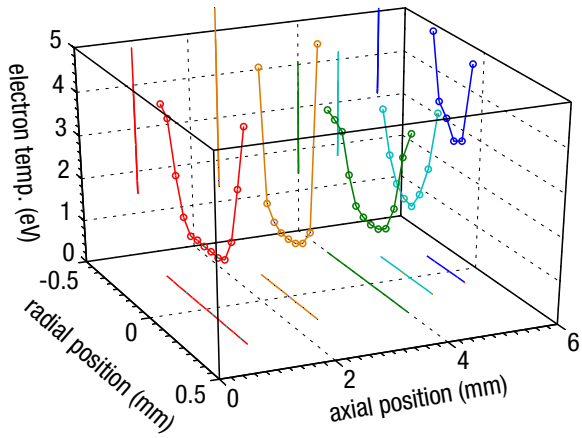

Figure 10. 2D profile of T_e of the plasma jet. An indication of the error bars is shown in figure 8.

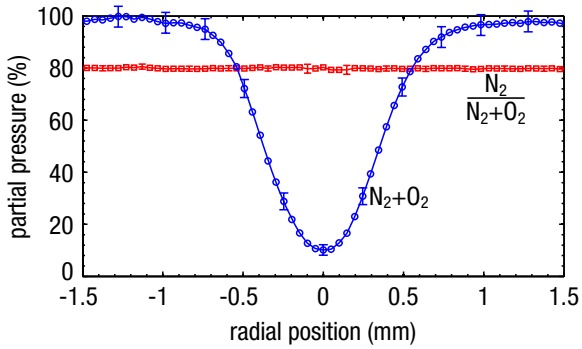

Figure 11. Partial pressures of $N_2 + O_2$ at 4.75 mm from the tube end.

can be explained by random movement of the plasma that can be seen by eye. The plasma width is about half the tube size, and close to the tube the plasma moves around in the flow. Further downstream, however, the plasma is more stabilized in the center of the argon flow. This means that close to the tube the plasma appears wider with lower n_e , but in fact it is an average of the moving plasma.

The partial pressure $p_{N_2+O_2}$ and the N_2/O_2 ratio are shown in figure 11. In the center it equals 9.7×10^3 Pa, which corresponds to 9.7vol%. The N_2/O_2 ratio fits very constantly to $(79.9/20.1 \pm 0.6)\%$ for each radial position. This means that the mixing ratio N_2/O_2 seems not to be influenced by the plasma. Figure 12 shows a 2D profile of the partial air pressure.

The temperatures determined by Rayleigh and Raman scattering are shown in figure 13, and 2D profiles in figure 14. Although in principle these represent two different temperatures—translational temperature of heavy particles (gas temperature) and rotational temperature of N_2 and O_2—they are often assumed to be equal at atmospheric pressure. Outside the plasma T_{rot} and T_g indeed match, but as the air concentration decreases toward the plasma center, T_{rot} is lower than T_g. It must be noted that the fitting method for Raman scattering yields a poor accuracy of T_{rot} in the cases with only a few percent of air. Nevertheless the measured difference between T_g and T_{rot} seems to be in some cases larger than the error of the fitting (figure 13).

A number of cases where $T_{rot} < T_g$ have been observed earlier. In CO it has been reported by Zikratov *et al* [22],

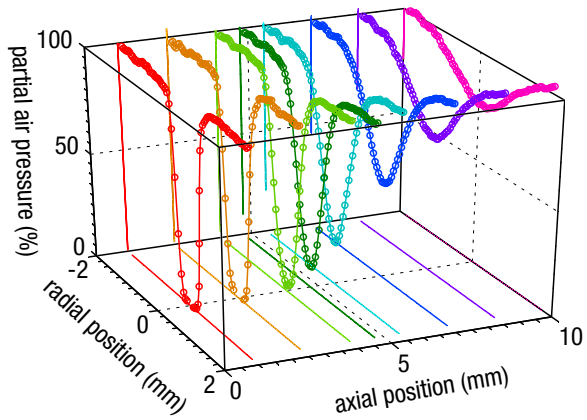

Figure 12. 2D profile of the partial air pressure ($N_2 + O_2$) in the plasma jet. An indication of the error bars is shown in figure 11.

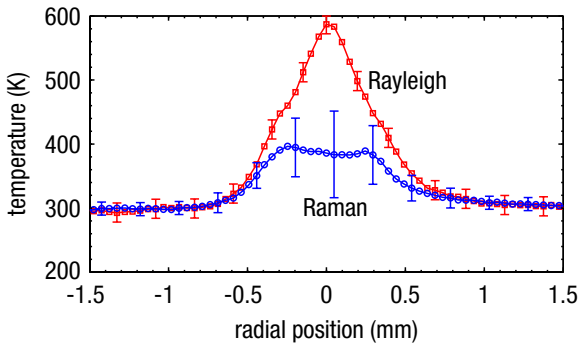

Figure 13. Radial profile of the gas temperature measured by Rayleigh scattering, and the rotational temperature of air measured by Raman scattering.

where ro-vibrational coupling of excited states of CO can lead to distortions of the rotational distributions. Another example is the ro-vibrational distribution of H_2 in cascaded arc plasmas as investigated by Gabriel *et al* [23]. Low T_{rot} has been found for ground state H_2, HD and D_2, probably due to association processes. Similar effects could be present in our case.

5. Discussion

5.1. Losses of vibrational ground state molecules

In the above treatment of Raman scattering the assumption has been made that all molecules are in the lowest vibrational state, and that there is no temperature dependence of the vibrational state distribution. In the case this assumption is not met, this would lead to a loss of molecules toward higher vibrational states, and thus to an underestimation of the molecular density. The ratio of the number of molecules n in the vibrational level $v = 1$ and $v = 0$ is given by [19]

$$\frac{n_1}{n_0} = \mathrm{e}^{-\frac{E_{10}}{k_B T_{vib}}}, \tag{14}$$

where E_{10} is the energy of the first vibrational band (1-0) (see table 1). For $T_{vib} = 1200\,\mathrm{K}$ (about twice the maximum gas temperature) this results in an underestimation of the N_2 and O_2 density of 6% and 15%, respectively. Due to the difference

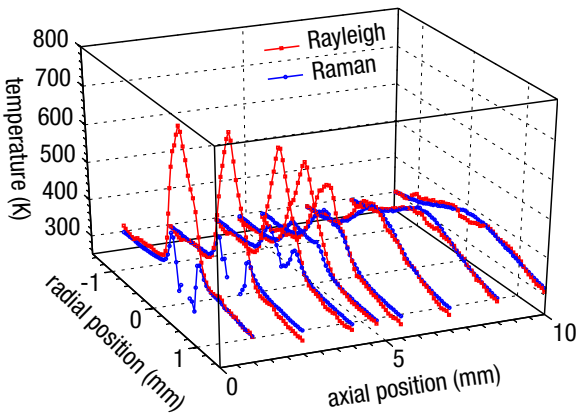

Figure 14. 2D profile of T_g and T_{rot} in the plasma jet.

between N_2 and O_2 the N_2/O_2 mixing ratio (normally 80/20%) would change to 81.6/18.4%. We do not observe such a change, which leads to the assumption that the vibrational temperature is lower and the vibrational loss is less. Indeed this is likely in our continuous discharge, as Filimonov *et al* [24] showed that exchange of rotational and vibrational energy happens on timescales of $10\,\mu s$ for the ground state of N_2. In our case the rate will be even faster, since the plasma operates at atmospheric pressure, and with higher n_e. The underestimation of the partial pressure then falls within the error margin (of about 10%, see figure 11), so we can in first approximation ignore this effect.

5.2. T_e increase at the edge

Radially at the edge of the plasma and axially at the end of the plasma n_e decreases and T_e increases. This has been observed previously by Palomares *et al* in a similar atmospheric pressure jet [5], as well as in a low pressure microwave plasma [25]. Jonkers *et al* [26] have studied the effects of air entrainment on n_e and T_e in an atmospheric pressure plasma torch of argon. It was found that when operating the plasma torch in an air environment the size is smaller (n_e decreases more rapidly at the edges) and T_e is higher than when the plasma operates in a pure argon environment. Indeed the 2D profiles in figures 9, 10 and 12 show that n_e decreases and T_e increases where $p_{N_2+O_2}$ increases.

5.3. Experimental detection limits

The lowest electron density at which pure Thomson scattering can be applied in these types of atmospheric plasmas is about $5 \times 10^{18}\,\mathrm{m}^{-3}$, mostly limited by the background signal caused by plasma emission and false stray light. This limit is higher than in the case of low pressure due to the fact that the plasma is smaller and the gradients in n_e and T_e are higher, so that only a small part of the iCCD is used for the actual plasma signal. At the same time the plasma emission and the Rayleigh signal are stronger, causing more background noise.

The lower limit for Raman scattering in atmospheric pressure plasmas is determined by the noise level due to the plasma background, which was found to correspond to an air percentage of about 1vol%.

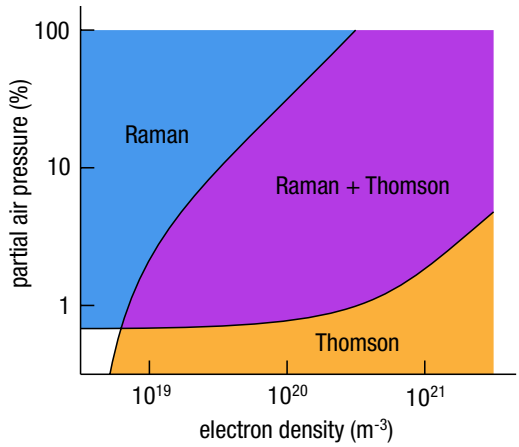

Figure 15. Parameter space in which Thomson and Raman scattering measurements can be applied.

To determine the limit of the described fitting method we compare the maximum intensities of the Thomson and the Raman signals. To have reliable values for the fitting parameters from both signals, the weakest signal of the two must be at least 10% of the strongest. This means that in a plasma with 10% air the lower limit for Thomson scattering is at about $n_e = 3 \times 10^{19}\,m^{-3}$. For $n_e = 10^{21}\,m^{-3}$ the lower limit for measuring Raman scattering is about 3%. The range in which Raman and Thomson scattering can be applied is illustrated in figure 15. Note that this figure only gives an indication, since these limits depend on other plasma parameters such as T_{rot} and T_e. Also the limits depend on experimental values such as the noise level and instrumental profile, which are specific for the setup.

6. Conclusion

The method presented in this paper makes it possible to acquire temperatures and densities of electrons and molecules from Thomson and Raman scattering experiments in Raman active gasses. This considerably increases the parameter space in which these methods can be applied. It is shown that it is possible to measure profiles with a high spatial resolution of 50 μm of n_e, T_e, n_{N_2}, n_{O_2} and T_{rot} simultaneously and including absolute calibration in one single measurement.

Electron densities in the range 10^{19}–$10^{21}\,m^{-3}$ are measured for air concentrations of 1–10% in argon in an atmospheric non-thermal microwave plasma jet.

Acknowledgments

The authors acknowledge the financial support of the Dutch Technology Foundation STW.

References

[1] Dorai R and Kushner M J 2003 A model for plasma modification of polypropylene using atmospheric pressure discharges *J. Phys. D: Appl. Phys.* **36** 666–85
[2] Fridman A 2008 *Plasma Chemistry* (Cambridge: Cambridge University Press)
[3] Laroussi M 2009 Low-temperature plasmas for medicine? *IEEE Trans. Plasma Sci.* **37** 714–25
[4] Kong M G, Kroesen G M W, Morfill G, Nosenko T, Shimizu T, van Dijk J and Zimmermann J L 2009 Plasma medicine: an introductory review *New J. Phys.* **11** 115012
[5] Palomares J M, Iordanova E I, Gamero A, Sola A and van der Mullen J J A M 2010 Atmospheric microwave-induced plasmas in Ar/H_2 mixtures studied with a combination of passive and active spectroscopic methods *J. Phys. D: Appl. Phys.* **43** 395202
[6] Marshall K A and Hieftje G M 1987 Measurement of true gas kinetic temperatures in an inductively coupled plasma by laser-light scattering. Plenary lecture *J. Anal. At. Spectrom.* **2** 567
[7] Muraoka K, Uchino K and Bowden M D 1998 Diagnostics of low-density glow discharge plasmas using Thomson scattering *Plasma Phys. Control. Fusion* **40** 1221–39
[8] van der Mullen J J A M, van de Sande M J, de Vries N, Broks B, Iordanova E I, Gamero A, Torres J and Sola A 2007 Single-shot Thomson scattering on argon plasmas created by the microwave plasma torch; evidence for a new plasma class *Spectrochim. Acta* B **62** 1135–46
[9] Belostotskiy S G, Khandelwal R, Wang Q, Donnelly V M, Economou D J and Sadeghi N 2008 Measurement of electron temperature and density in an argon microdischarge by laser Thomson scattering *Appl. Phys. Lett.* **92** 221507
[10] Gregoric G, Schein J, Schwendinger P, Kortshagen U, Heberlein J and Pfender E 1999 Thomson scattering measurements in atmospheric plasma jets *Phys. Rev.* E **59** 2286–91
[11] Belostotskiy S G, Wang Q, Donnelly V M, Economou D J and Sadeghi N 2006 Three-dimensional gas temperature measurements in atmospheric pressure microdischarges using Raman scattering *Appl. Phys. Lett.* **89** 251503
[12] Vaughan G, Wareing D P, Pepler S J, Thomas L and Mitev V 1993 Atmospheric temperature measurements made by rotational Raman scattering *Appl. Opt.* **32** 2758–64
[13] Narishige S, Kitamura S, Sakemi S, Tomita K, Uchino K, Muraoka K and Sakoda T 2002 Thomson scattering diagnostics of glow discharge plasmas produced in Raman active gases *Japan. J. Appl. Phys.* **41** L1259–62
[14] Kempkens H and Uhlenbusch J 2000 Scattering diagnostics of low-temperature plasmas (Rayleigh scattering, Thomson scattering, CARS) *Plasma Sources Sci. Technol.* **9** 492–506
[15] van de Sande M J 2002 Laser scattering on low temperature plasmas—high resolution and stray light rejection *PhD Thesis* Eindhoven University of Technology
[16] Sneep M and Ubachs W 2005 Direct measurement of the Rayleigh scattering cross section in various gases *J. Quant. Spectrosc. Radiat. Transfer* **92** 293–310
[17] Sutton J A and Driscoll J F 2004 Rayleigh scattering cross sections of combustion species at 266, 355, and 532 nm for thermometry applications *Opt. lett.* **29** 2620–2
[18] Penney C M, St Peters R L and Lapp M 1974 Absolute rotational Raman cross sections for N_2, 0_2, and CO_2 *J. Opt. Soc. Am.* **64** 712–16
[19] Herzberg G 1950 *Molecular Spectra and Molecular Structure: I. Spectra of Diatomic Molecules* 2nd edn (New York: van Nostrand)
[20] Takamura S, Saito S, Kushida G, Kando M and Ohno N 2010 Fluid mechanical characteristics of microwave discharge jet plasmas at atmospheric gas pressure 2010 *IEEJ Trans. Fundam. Mater.* **130** 493–500
[21] Lagarias J C, Reeds J A, Wright M H and Wright P E 1998 Convergence properties of the Nelder–Mead simplex method in low dimensions *SIAM J. Optim.* **9** 112
[22] Zikratov G, Setser D W and Sadeghi N 2000 Spectroscopy and relaxation kinetics of the perturbed CO($b\,^3\Sigma^+$,$v = 0,1,2$) and CO($a\,^3\Sigma+$, $v = 3136$, 40, and 41) levels and

reinterpretation of CO($a\,^3\Sigma+$, $v = 34$ and 35) formation in the Kr(5s[1/2]$_0$)+CO reaction *J. Chem. Phys.* **112** 10845

[23] Gabriel O, van den Dungen J J A, Schram D C and Engeln R 2010 Nonequilibrium rovibrational energy distributions of hydrogen isotopologues in an expanding plasma jet *J. Chem. Phys.* **132** 104305

[24] Filimonov S and Borysow J 2007 Vibrational and rotational excitation within the $X\,^1\Sigma$ state of N_2 during the pulsed electric discharge and in the afterglow *J. Phys. D: Appl. Phys.* **40** 2810–17

[25] Palomares J M, Iordanova E I, van Veldhuizen E M, Baede L, Gamero A, Sola A and van der Mullen J J A M 2010 Thomson scattering on argon surfatron plasmas at intermediate pressures: Axial profiles of the electron temperature and electron density *Spectrochim. Acta* B **65** 225–33

[26] Jonkers J, Selen L J M, van der Mullen J J A M, Timmermans E A H and Schram D C 1997 Steep plasma gradients studied with spatially resolved Thomson scattering measurements *Plasma Sources Sci. Technol.* **6** 533